ISSN 2070-2051, Protection of Metals and Physical Chemistry of Surfaces, 2021, Vol. 57, No. 1, pp. 59–67. © Pleiades Publishing, Ltd., 2021.
Russian Text © The Author(s), 2021, published in Fizikokhimiya Poverkhnosti i Zashchita Materialov, 2021, Vol. 57, No. 1, pp. 65–73.

NANOSCALE AND NANOSTRUCTURED MATERIALS AND COATINGS

A Study of the Composition and Structure of a Solid Electrolyte Interface (SEI) Formed on the Surface of Electrode Material Based on SnO_x/Sn@MWCNT Nanocomposite

P. M. Korusenko[a, b, *], S. N. Nesov[a], V. V. Bolotov[a], S. N. Povoroznyuk[a], and E. O. Fedorovskaya[c]

[a] *Omsk Scientific Center, Siberian Branch, Russian Academy of Sciences, Omsk, 644024 Russia*

[b] *Omsk State Technical University, Omsk, 644050 Russia*

[c] *Research Group of Electrochemical Energy Conversion and Storage, Department of Chemistry, School of Chemical Technology, Aalto University, P.O. Box 16100, FI-00076 Finland*

**e-mail: korusenko_petr@mail.ru*

Received March 14, 2020; revised May 4, 2020; accepted May 12, 2020

Abstract—In the process of the performed studies, new information has been obtained about the composition and structure of the solid electrolyte interface (SEI) formed on the surface of electrodes based on the initial composite SnO_x@MWCNT (tin oxide/multiwall carbon nanotubes) and the SnO_x/Sn@MWCNT composite formed by irradiation using a pulsed ion beam of nanosecond duration. It has been shown that, after long cycling of electrode based on an irradiated composite (SnO_x/Sn@MWCNT), the tin concentration remained approximately at the same level. This result indicated high interphase adhesion of the metal–oxide component to the surface of MWCNTs in the irradiated composite. Using X-ray photoelectron spectroscopy methods, it has been established that the SEI layer formed under these conditions consisted predominantly of lithium carbonate and oxide and organic compounds comprising products of interaction of solvents (ethylene carbonate and dimethyl carbonate) of the electrolyte with the electrode surface. It has been found that the electrode based on the irradiated composite demonstrates the best electrochemical characteristics as a material for the electrodes of lithium-ion batteries.

Keywords: electrodes, solid electolyte interface (SEI), composites, multiwall carbon nanotubes, SnO_x/Sn nanoparticles with core–shell structure, X-ray spectroscopy methods (XPS, NEXAFS), synchrotron radiation, electrical impedance spectroscopy

DOI: 10.1134/S2070205121010135

1. INTRODUCTION

At present, one of the most promising devices for energy storage and conversion is represented by lithium-ion batteries (LIBs), in which graphite of a theoretical specific capacity of 372 mA h g^{-1} is used as the anode material [1]. Promising materials for the production of LIB anodes include tin metal (Sn) and tin oxide (SnO_2), which have specific capacities of ~991 and 790 mA h g^{-1}, respectively [1]. A high value of the specific capacity of these materials is achieved by the ability to form intermetallic phases Li_xSn ($0 \le x \le 4.4$) [1, 2]. However, changes of the tin volume of up to 250–300% during the lithiation/delithiation process (introduction and removal of lithium ions) during charge–discharge cycles resulted in instability of the material and its performance degradation [1, 3]. Tin oxide nanoparticles were used to reduce the effect of volume changes, cracking, and tin detachment and, consequently, to decrease the degradation of the electrochemical characteristics of the electrodes during charging/discharging process [4]. In particular, a number of works [5–7] demonstrated the prospects of using Sn/SnO_2 nanoparticles with a core–shell structure for LIBs. The specific capacity of this material was in the range of 790–991 mA h g^{-1} depending on the "shell" thickness (SnO_x), which prevented oxidation of the "core" (Sn). In addition, the decrease of the "shell" thickness down to several nanometers can significantly decrease the irreversible capacitance related to the formation of Li_2O and increase the ratio of Sn to Li_2O in the anode matrix [5–7]. However, the degradation of the electrochemical properties of electrodes based on Sn/SnO_2 nanoparticles ranged from 68 to 96% after 30 charge/discharge cycles, which limits their practical use as LIB anodes. One of the approaches to reduce the negative effects of coagulation of Sn/SnO_2 nanoparticles and their detachment from the current-collecting substrate during the cyclic charge/discharge process was to deposit Sn/SnO_2 on carbon nanotubes (multiwalled carbon nanotubes

(MWCNTs)) [7–9]. The framework of carbon nanotubes is capable to minimize the effect of changes in the volume of metal oxide nanoparticles during the cyclic processes of lithiation/delithiation due to its flexibility. In addition, carbon nanotubes had low electrical resistance, which contributed to the improvement of charge transfer in charge/discharge cycles. A study of electrochemical characteristics showed that such composites as SnO_x/Sn@MWCNT had high specific capacity in the first charge/discharge cycle up to ~2100 mA h g^{-1}, the value of which remained at the level of ~400–800 mA h g^{-1} after 30 cycles [7–9].

One important factor affecting the performance of advanced LIBs consists in the peculiarities of formation of the electrolyte's solid phase on the surface of electrode materials [10, 11]. This layer is formed at the electrode–electrolyte interface during the first several charge/discharge cycles. One of its functions is to prevent further reduction of the electrolyte to maintain the required service life and performance of the LIBs [10]. Despite the large number of studies that have been carried out in this area, there are still open questions related to understanding the mechanisms of formation of the solid electrolyte interface (SEI) layer and its composition and structure depending on the electrode material and organic solvents as well as additives used in the electrolyte composition [11–13].

Earlier, the authors suggested an original method of formation of a SnO_x/Sn@MWCNT nanocomposite with a core–shell metal oxide component structure based on the high-energy effect of a pulsed ion beam (PIB) [14]. It was shown that the use of a PIB to modify the initial composite SnO_{2-x}@MWCNT obtained by a simple chemical vapor deposition (CVD) method enabled one to form structural defects and oxygen-containing groups on the outer walls of MWCNTs and homogeneously dispersed Sn/SnO_x nanoparticles on the surface of nanotubes within one irradiation cycle.

The objective of the present work was to obtain information about the composition and structure of the SEI layer and electrochemical properties of electrodes based on the initial and modified nanocomposites using scanning electron microscopy (SEM), energy-dispersive X-ray spectroscopy EDX, X-ray photoelectron spectroscopy (XPS), and near edge X-ray absorption fine structure (NEXAFS). The initial and irradiated nanocomposites were studied by means of electrochemical impedance spectroscopy (EIS).

2. EXPERIMENTAL

MWCNT layers were formed by the CVD method at pyrolysis of a mixture of acetonitrile and ferrocene (100 : 1) on Si/SiO_2 substrates with a surface oxide layer thickness of ~100 nm. Synthesis of MWCNTs was conducted at 800°C for 30 min. The thickness of the grown MWCNT layers was ~15 ± 3 μm.

The SnO_x@MWCNT nanocomposite was produced by means of hydrolysis and thermal decomposition of $SnCl_2 \cdot 2H_2O$ compound of a weight of 0.6 g in a CVD reactor at 380°C with subsequent vapor deposition on a Si/SiO_2 substrate heated to 240°C with a bulk of MWCNT. Modification of the SnO_x@MWCNT nanocomposite was performed by a PIB using a TEMP-4M accelerator (15% H^+, 85% C^+, ion energy of 250 keV, pulse of duration of 120 ns) [15] through triple irradiation at an energy density of 0.5 J/cm^2.

Preparation of electrodes for structural and electrochemical studies was carried out in several stages. At the first stage, the nanocomposite layer or the initial MWCNTs were removed from the Si/SiO_2 substrate by a medical blade. The powder obtained in this way was later used as an active material in the production of work electrodes. The second stage comprised the mixing of 85 wt % of active material, 5 wt % of highly conductive carbon, and 10 wt % of the binding material—polyvinylidene difluoride (PVDF)—with the addition of an organic solvent N-methyl-2-pyrrolidone (NMP) and subsequent thorough mixing for 10 min. The resulting suspension was deposited on a copper foil of a 10-μm thickness and then dried at 80°C for 12 h in a vacuum (~10^{-2} Torr) to remove NMP residues.

A half-cell based on the CR2032 battery was used to measure the electrochemical characteristics of electrode materials. Plates made of metal lithium were used as a counterelectrode. One molar solution of $LiPF_6$ in a mixture of ethylene carbonate (EC) and dimethyl carbonate (DMC) and the ratio of 1 : 1 was used as an electrolyte. The assembly of half-cells was carried out in a dry argon atmosphere in a glove box at a water vapor concentration of <5 ppm.

The measurement of electrochemical characteristics of the electrodes was conducted in a galvanostatic mode at a constant current density of 100 mA h g^{-1} using an A211-BTS-35-1U potentiostat-galvanostat station. The working electrodes were first discharged in a galvanostatic mode in the voltage range from 3.0 to 0.1 V (lithiation) and then charged to a voltage of 3.0 V (delithiation) relatively to Li/Li^+. EIS half-cell measurements were performed by an Elins P-45X electrochemical workstation using the frequency response analysis. The impedance spectra were obtained in the frequency range from 0.01 to 100000 Hz.

To study the morphology and chemical composition of the work electrodes, SEM and EDX methods implemented on a JEOL JSM 6610 LV scanning electron microscope at the Omsk Regional Shared Equipment Center SB RAS were used. During SEM measurements, the energy of the initial electron beam was 20 keV. The study of the atomic and electronic structure of the surface layers of the electrodes was con-

Table 1. Quantitative EDX analysis of electrodes based on the initial and irradiated composites before cycling

Point number	Concentration, at %						
	[C]	[O]	[F]	[P]	[Cl]	[Cu]	[Sn]
Initial composite (SnO_x@MWCNT)							
Point 1	55.13	29.94	9.62	1.69	0.21	1.80	1.61
Point 2	74.66	12.71	4.00	0.74	0.20	1.34	6.35
Point 3	60.05	27.52	6.65	1.63	0.14	1.30	2.71
Average	63.28	23.39	6.75	1.35	0.18	1.48	3.55
Irradiated composite (SnO_x/Sn@MWCNT)							
Point 1	53.76	15.87	24.79	0.58	0.16	0.48	4.36
Point 2	76.67	3.51	13.25	0.27	0.19	0.56	5.55
Point 3	53.92	20.68	19.05	0.39	0.15	0.50	5.31
Average	61.45	13.35	19.03	0.41	0.16	0.51	5.07

ducted using the NEXAFS and XPS methods implemented by means of synchrotron radiation of a BESSY II electron storage ring (Berlin, Germany) on the equipment of the Russian–German channel (RGBL) of the RGL-PES station. The pressure of residual gases in the measurement chamber was ~2×10^{-10} Torr. XPS spectra of lithium (Li 1s) were obtained at a photon energy of 150 eV using a PHOIBOS 150 hemispherical analyzer with a transmission energy value of 15 eV. The escape depth of the photoelectrons for XPS was ~5 nm. NEXAFS carbon spectra were obtained by measuring the leakage current from the sample. The monochromator resolution in the energy range of the K edge of carbon absorption at ~285 eV was ~70 meV. The analysis depth by NEXAFS was ~15 nm. The structure of the initial electrodes (without contact with the electrolyte) and that after the first charge/discharge cycle and long-duration cycling (30 charge/discharge cycles) were studied. In order to conduct SEM, EDX, XPS, and NEXAFS studies of the electrode structure after lithium intercalation/deintercalation, the half-cells were disassembled in a glove box in an argon medium. To remove the electrolyte residues, all the electrodes were washed in dimethyl carbonate (DMC) and remained in the glove box in an argon medium for 12 h.

3. RESULTS AND DISCUSSION

3.1. Analysis of Morphology and Chemical Composition

Figure 1 shows SEM images of electrodes based on the initial and irradiated composite before and after cycling. One can observe that the electrode surface before cycling was porous and contained mainly MWCNTs with a metal oxide component. In the case of an electrode formed from the initial composite, tin oxide clusters with a size of ~100 nm were observed (Fig. 1a), while the size of metal oxide clusters was less than 40 nm and they were more homogeneously distributed over the MWCNTs surface in an electrode made of an irradiated composite (Fig. 1b). The results of the EDX analysis demonstrated that the electrodes contained the following chemical elements before cycling: [C], [O], [F], [Cl], [Cu], and [Sn] (Table 1). The presence of fluorine was related to the presence of polyvinylidene fluoride (binder), while that of copper was related to the signal from the current-collecting substrate of the electrodes. Quantitative analysis showed that the electrodes had almost the same tin content.

Analysis of SEM images of the electrodes after cycling shows that the electrode surface changed significantly as compared to the initial electrodes (Figs. 1c, 1d). This was the result of the interaction of the electrodes with the electrolyte and the formation of a SEI layer at the electrode-electrolyte interface. A sufficiently high depth of analysis by the EDX method (up to 10 μm) enabled one to evaluate the tin concentration change under the formed SEI layer (Table 2). One can observe that the tin concentration in the electrode based on the initial composite significantly decreased, while this value actually did not change for the electrode based on the irradiated composite. The decrease of the tin concentration in the electrode from the initial composite related to the removal of tin oxide clusters from the MWCNTs surface in cyclic charge/discharge processes, which must be determined by the low interfacial adhesion of tin clusters to the nanotube surface. In the case of an electrode made of an irradiated composite, the preservation of the tin concentration can be explained by an increase of interfacial adhesion at the MWCNT–metal oxide component interface as a result of the formation of defects and functional oxygen-containing groups on the MWCNTs surface under the effect of a PIB, as well as by decrease in the characteristic size of metal oxide clusters and their homogeneous distribution over the MWCNTs surface [16].

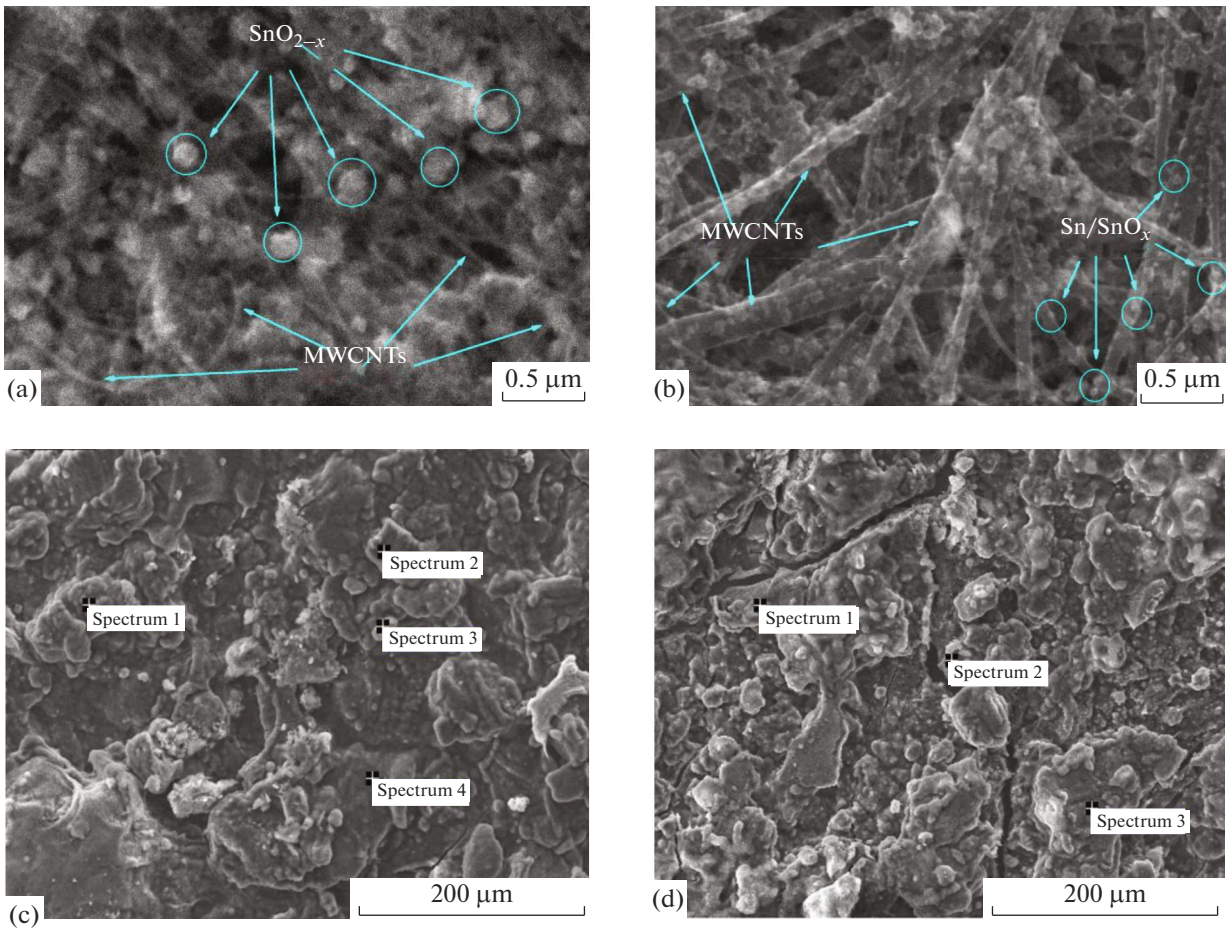

Fig. 1. SEM images of the electrode surface before cycling: (a) SnO_x@MWCNT, (b) SnO_x/Sn@MWCNT composite after irradiation by PIB and electrodes after cycling: (c) initial composite SnO_x@MWCNT, (d) composite after irradiation SnO_x/Sn@MWCNT.

3.2. Analysis of Local Atomic and Electronic Structure

Figure 2 shows the NEXAFS carbon spectra of electrodes formed on the basis of the initial and irradiated composites after different cycling stages. One can observe that the spectra of the initial electrodes contained intensive maxima at ~285 and ~291 eV, which corresponded to the π* and σ* states of sp^2-hybridized carbon [16, 17]. The shape of the carbon spectra indicated the preservation of the MWCNTs wall structure after production of work electrodes (Fig. 2, curve *1*). The presence of low-intensity states in the energy range of 286–290 eV indicated the presence of a certain amount of functional groups on the MWCNTs surface [16–18]. One can observe that the shape of the electrode spectra did not actually change after the first charge/discharge cycle (Fig. 2, curve *2*). This indicated the resistance of the MWCNTs surface to the effect of the electrolyte. The spectra of the electrodes significantly differed from those of the initial electrodes after long-duration cycling (Fig. 2, curve *3*). This must be the result of the presence of an SEI layer containing lithium oxides and fluorides on the electrode surface. The formation of the SEI layer is confirmed by the results of the analysis of the charge and discharge curves obtained by us earlier in [16]. Here, the presence of a high-intensity maximum corresponding to $-CO_3$ groups (~290 eV) in the spectra of cycled electrodes [17] could indicate to the presence of Li_2CO_3 in the composition of SEI layer. The presence of a low-intensity maximum corresponding to π*(C=C) states of carbon indicated the preservation of the MWCNTs structure after cycling.

Figure 3 shows the XPS spectra of lithium for electrodes based on the initial and irradiated composites after the 1st and 30th charge/discharge cycles. One can observe that the spectra had actually the same shape for both electrodes. Therefore, one can conclude that the SEI layer had an identical composition in both electrodes. According to the literature data, low-energy states at the binding energy of ~55 eV corresponded to lithium oxide [19, 20]. High-energy states at the binding energy of ~56 eV corresponded to

Table 2. Quantitative EDX analysis of electrodes based on the initial and irradiated composites after 30 charge/discharge cycles

Point number	Concentration, at %						
	[C]	[O]	[F]	[P]	[Cl]	[Cu]	[Sn]
Initial composite (SnO_x@MWCNT)							
Point 1	28.52	55.98	13.71	0.79	0.08	0.24	0.68
Point 2	25.21	67.08	5.40	0.68	0.12	0.29	1.22
Point 3	22.53	58.91	15.81	0.60	0.09	0.26	1.80
Point 4	26.89	63.80	6.93	0.99	0.12	0.38	0.89
Average	25.78	61.44	10.46	0.76	0.10	0.29	1.14
Irradiated composite (SnO_x/Sn@MWCNT)							
Point 1	14.83	48.26	30.14	1.61	0.17	0.81	4.18
Point 2	21.95	51.64	17.63	2.25	0.21	1.46	4.86
Point 3	16.46	34.58	41.85	1.88	0.16	0.90	4.17
Average	17.74	44.82	29.87	1.91	0.18	1.05	4.40

Table 3. EIS data

Electrode	R_f, Ω	R_{ct}, Ω	Slope of curve, deg	i_0, mA cm^{-2}
Initial composite	6.4	17.0	51	0.34
Irradiated composite	9.2	4.4	35	1.32
MWCNTs	6.7	63.7	19	0.40

lithium in bonds with fluorine (LiF) and lithium in carbonate (Li_2CO_3) [19, 20]. The presence of Li_2CO_3 correlated to the NEXAFS data.

Figure 4 shows the Sn spectra of the $M_{5,4}$ edge of absorption for electrodes based on the initial and irradiated composites. The spectrum of the M edge of tin for the electrode based on the initial composite (Fig. 4, curve *1*) was actually identical to the spectrum of the SnO_2 crystal powder with a tetragonal crystal lattice [16, 18]: clear maxima A, B, C, D, and E were observed. At the same time, the spectrum of the electrode based on the initial composite showed the A_1 feature at the photon energy of ~ 487 eV, which corresponded to oxygen vacancies in tin oxide. Therefore, it can be stated that the tin oxide in the electrode based on the initial composite was in the crystalline state and had an oxygen deficiency (SnO_{2-x}) [16, 18]. In the Sn spectrum of $M_{5,4}$ edge of the electrode based on a composite irradiated by PIB, the fusion of resonances A, B (M_5 edge) and D, E (M_4 edge) and significant increase of the intensity of the A_1 feature were observed (Fig. 4, curve *2*). The fusion of the main resonances in the Sn spectrum of $M_{5,4}$ edge of the irradiated composite related to the presence of signals from the Sn metal "core" and the SnO_x oxide "shell" of Sn/SnO_x nanoparticles [16]. Since the signal from the tin located under the formed SEI layer was weak, no studies were performed for both electrodes after the 1st and 30th charge/discharge cycles.

3.3. Study of Electrochemical Characteristics

Figure 5 presents the impedance hodographs in Nyquist coordinates for electrodes formed on the basis of the initial and irradiated composites and MWCNTs. The beginning of semicircles of hodographs in the high-frequency range corresponded to the resistance of the SEI layer and/or contact resistance R_f [21]. The radius of the semicircle is related to charge transfer resistance R_{ct} at the electrode/electrolyte interface [8, 21]. The low-frequency range of the hodograph corresponded to the Warburg impedance related to the diffusion of Li ions into the electrode [8, 21]. The kinetic parameters of the electrodes are shown in Table 3.

To analyze the hodographs of the electrode impedance, an equivalent scheme was used shown in the box in Fig. 5a. The validity test of the selected equivalent circuit was performed on an electrode based on MWCNTs by means of the EC-LAB software package, which enabled one to analyze impedance graphs. One can observe (Fig. 5b) that the approximating curve simulating the equivalent scheme obtained by means of the EC-LAB software package described adequately the experimental curve, which confirmed

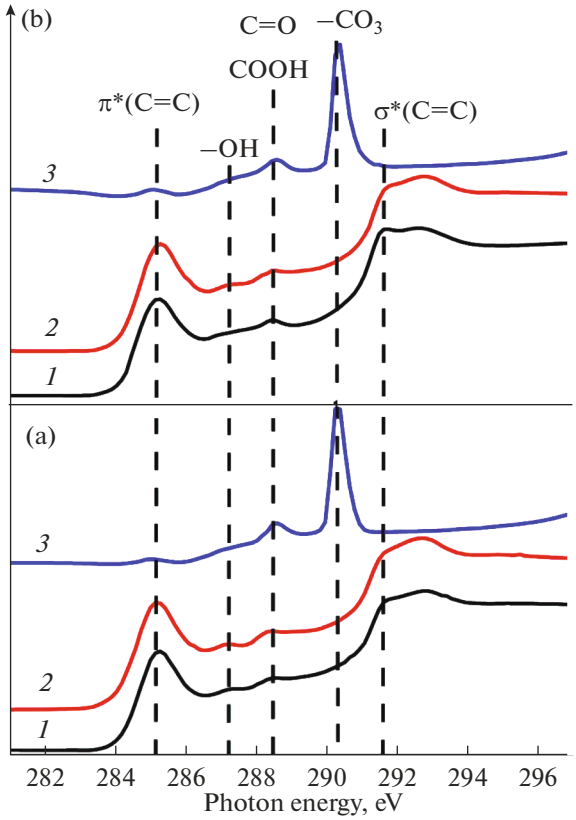

Fig. 2. NEXAFS spectra of the K edge of carbon absorption of electrodes obtained on the basis of initial composite SnO_x@MWCNT (a) and the SnO_x/Sn@MWCNT composite after irradiation of (b): (*1*) initial electrodes, (*2*) electrodes after the first charge/discharge cycle, and (*3*) electrodes after the 30th charge/discharge cycle.

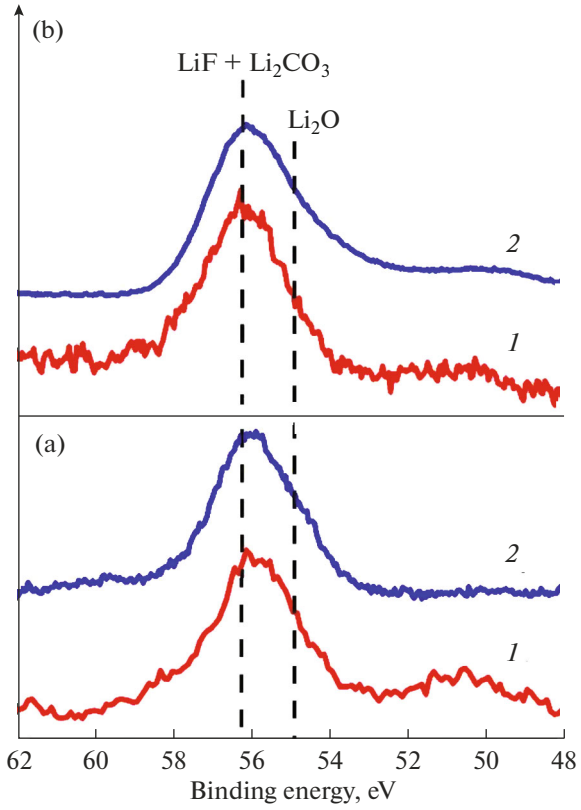

Fig. 3. XPS spectra of 1s lithium of electrodes obtained on the basis of the (a) initial SnO_x@MWCNT composite and (b) SnO_x/Sn@MWCNT composite after irradiation of (*1*) electrodes after the first charge/discharge cycle; (*2*) electrodes after the 30th charge/discharge cycle.

the validity of the selected equivalent scheme. R_f corresponded to the SEI layer resistance and/or contact resistance. CPE and R_{ct} comprised a constant phase element that simulated the behavior of a double layer of an imperfect condenser at the electrode-electrolyte interface and the charge transfer resistance, respectively. Warburg impedance Z_w was related to the diffusion of lithium ions into the electrode volume. Exchange current density i_0 can be calculated with to the equation $i_0 = RT/nFR_{ct}$, where R is the gas constant, T is the absolute temperature, n is the number of transferred electrons, and F is the Faraday constant [22].

Decomposition of an electrolyte is known [22] to be highly depending on the surface properties of electrode materials. Therefore, the higher R_f value for an electrode based on the irradiated composite was related to more advanced decomposition of the electrolyte on the surface of Sn/SnO_x nanoparticles as the result of the amorphous state of the oxide shell of these nanoparticles and to a higher degree of deficiency in the walls of carbon nanotubes.

As shown in Figure 5a and data of Table 3, the R_{ct} value for the electrodes based on the initial (17 Ω) and irradiated composites (4.4 Ω) was significantly lower than the value of the charge transfer resistance of the electrode based on MWCNTs (63.7 Ω). These results indicated the formation of a more conductive SEI layer in the case of the use of composite electrodes. The lowest R_{ct} value for an irradiated composite electrode might indicate the maintenance of good electronic contact between Sn/SnO_x and nanoparticles after lithium intercalation/deintercalation, as a result of a stronger interfacial adhesion determined by the presence of defects and functional groups on the MWCNTs surface.

As is shown in Fig. 5c, the lines of dependence of the Warburg impedance on the inverse square root of the angular frequency had actually similar slope [23], which indicated similar values of the Warburg coefficients and, accordingly, similar values of the lithium diffusion coefficients in composite-based electrodes. However, as shown in Table 3, a higher value of exchange current i_0 was observed for an electrode based on the irradiated composite, which indicated high rate of electrochemical reactions [22]. This must

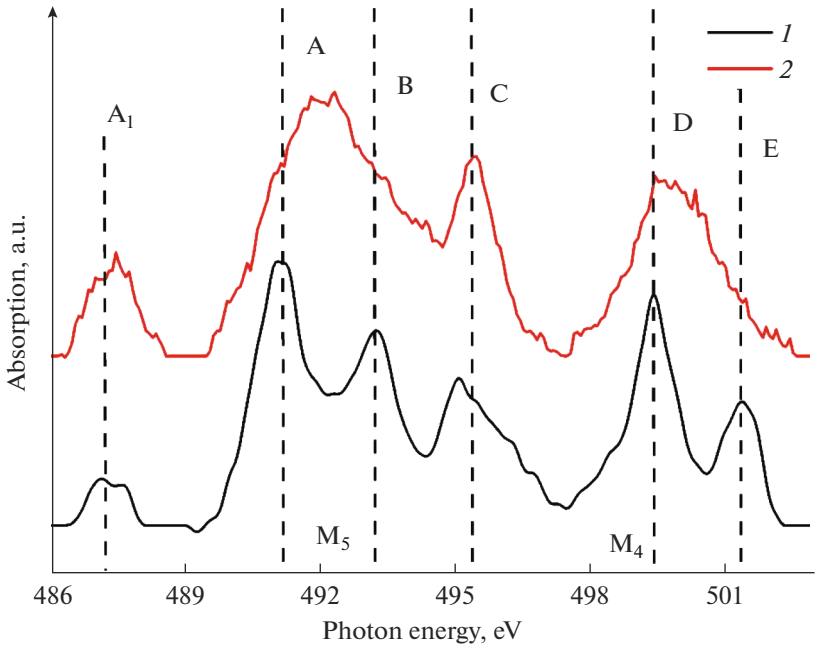

Fig. 4. NEXAFS spectra of the M edge of tin absorption of initial electrodes obtained on the basis of the (*1*) initial composite SnO_x@MWCNT and (*2*) SnO_x/Sn@MWCNT composite after irradiation.

be caused by the unique architecture of Sn/SnO_x particles. We believe that the nanoparticle shell was completely converted to Li_2O at the first charge/discharge cycle, and the subsequent formation of Li_xSn_y phases when Li ions were introduced into the nanoparticle core proceeded without additional consumption of lithium ions for SnO_x reduction.

To sum up, the presented results show that the irradiated composite electrode had the best electrochemical characteristics, which were provided by high interfacial adhesion between functionalized MWCNTs and Sn/SnO_x nanoparticles and unique architecture of these nanoparticles.

4. CONCLUSIONS

A comparative study of the composition and structure of electrode materials for lithium-ion batteries based on the initial SnO_x@MWCNT composite and SnO_x/Sn@MWCNT composite with a "core–shell" structure formed using a pulsed ion beam has been performed by means of a complex of SEM, EDX, XPS, and NEXAFS methods of analysis. Data on the effect of cyclic intercalation/deintercalation processes of lithium on changes in the structure and chemical state of the electrodes have been obtained. It has been established that long-duration cycling of the electrode from the initial composite results in a significant decrease of the tin concentration in the electrode, while the amount of tin actually did not change in the electrode from the irradiated composite. This indicates the stability of the composite modified by a pulsed ion beam to degradation processes as a result of the increased adhesion of the metal oxide component to the MWCNTs surface. Analysis of the electrode surface after cycling enabled one to determine the composition of the groups included in the SEI layer. It has been established that the SEI layer formed under these conditions consisted mainly of Li_2CO_3, Li_2O, and organic compounds that were products of interaction of electrolyte solvents (DMC, EC) with the electrode surface. It has been shown that the electrode based on the irradiated composite demonstrates the best electrochemical characteristics as a material for the LIB electrode, which was caused by high interfacial adhesion between functionalized MWCNTs and Sn/SnO_x nanoparticles and unique architecture of these nanoparticles.

ACKNOWLEDGMENTS

The authors are grateful to the staff of the Omsk Scientific Center of the Siberian Branch of the Russian Academy of Sciences: to Yu.A. Sten'kin for the synthesis of MWCNT assemblies and to K.E. Ivlev for the formation of composites by the CVD method, as well as to A.I. Pushkarev, a staff member of Tomsk Polytechnic University, for irradiation of the composite samples by a PIB. The authors also grateful to management of the Omsk Regional Shared Equipment Center SB RAS for providing equipment for sample analysis by the SEM and EDX methods and to the administration of the Russian-German channel of the BESSY II synchrotron storage for assistance in conducting studies by the XPS and NEXAFS methods.

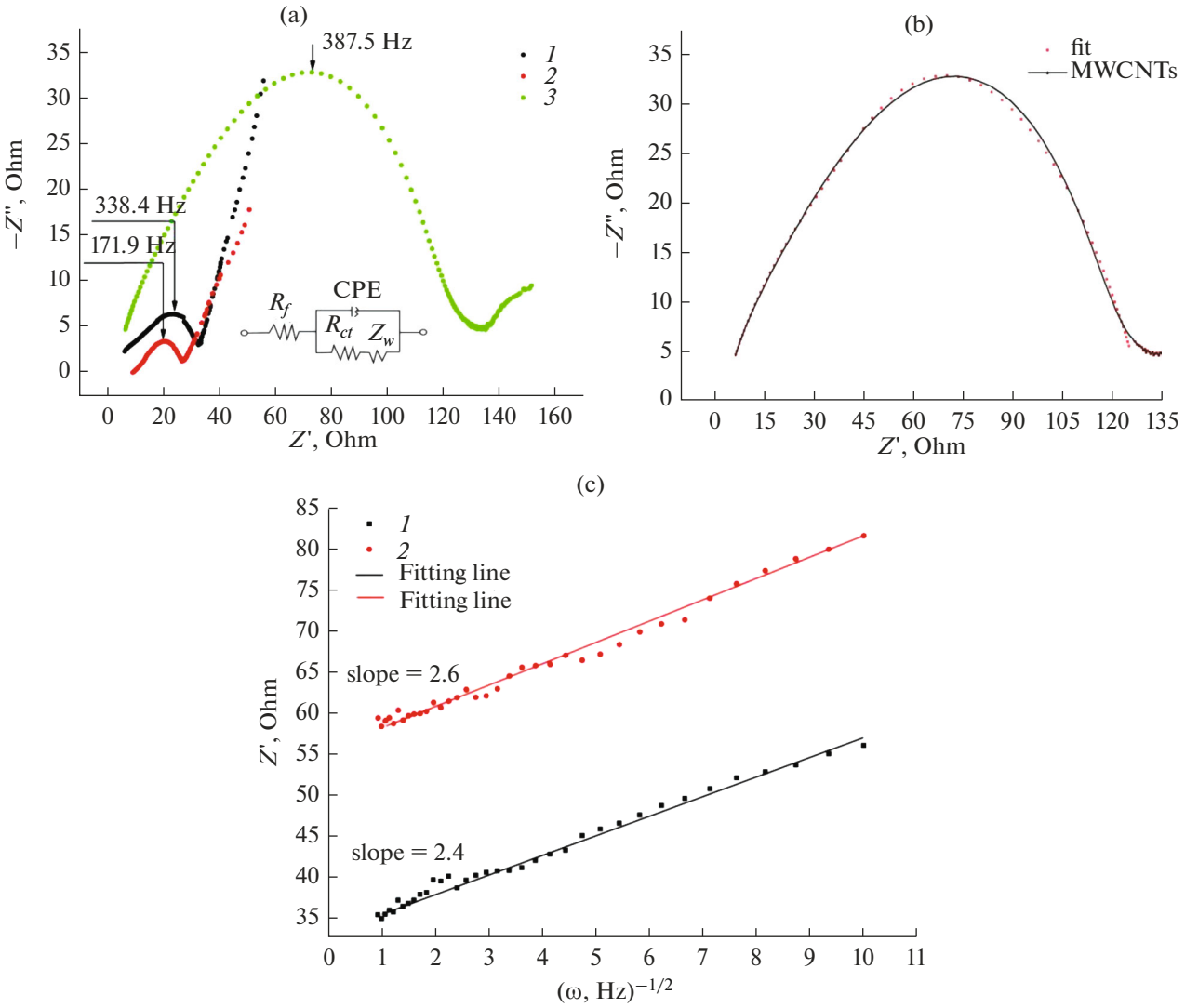

Fig. 5. (a) Impedance hodographs in Nyquist coordinates for electrodes after cycling: based on the (*1*) initial composite SnO_x@MWCNT, (*2*) SnO_x/Sn@MWCNT composite after irradiation, and (*3*) MWCNTs. (b) Comparison of the experimental impedance hodograph in Nyquist coordinates for an electrode based on MWCNTs and an approximation curve simulating an equivalent circuit. (c) Graph of dependence Z' on the square root of the angular frequency ($\omega^{-1/2}$) for an electrode based on the (*1*) initial composite SnO_x@MWCNT and (*2*) composite SnO_x/Sn@MWCNT after irradiation.

FUNDING

The work was carried out according to the state task of the Omsk Scientific Center SB RAS "Investigation of physical processes in heterostructures based on new functional nanomaterials and nanocomposites for microsensors, chemical current sources and medical applications."

REFERENCES

1. Chen, J., *Materials,* 2013, vol. 6, p. 156.
2. Osiak, M., Geaney, H., Armstrong, E., et al., *J. Mater. Chem. A,* 2014, vol. 2, p. 9433.
3. Ren Zong, H., Hui, L., Mei Qin, Z., et al., *Chin. Sci. Bull.,* 2012, vol. 57, p. 4119.
4. Hu, R., Sun, W., Liu, H., et al., *Nanoscale,* 2013, vol. 5, p. 11971.
5. Osiak, M.J., Armstrong, E., Kennedy, T., et al., *ACS Appl. Mater. Interfaces,* 2013, vol. 5, p. 8195.
6. Wang, X.-L., Feygenson, M., Aronson, M.C., et al., *J. Phys. Chem. C,* 2010, vol. 114, p. 14697.
7. Alaf, M. and Akbulut, H., *J. Power Sources,* 2014, vol. 247, p. 692.
8. Alaf, M., Tocoglu, U., Kayis, F., et al., *Fullerenes, Nanotubes, Carbon Nanostruct.,* 2016, vol. 24, p. 630.
9. Liu, C., Huang, H., Cao, G., et al., *Electrochim. Acta,* 2014, vol. 144, p. 376.
10. Veith, G.M., Mathieu, D., Sacci, R.L., et al., *Sci. Rep.,* 2017, vol. 7, p. 6326.

11. Gauthier, M., et al., *J. Phys. Chem. Lett.,* 2015, vol. 6, p. 4653.

12. Nie, M., et al., *J. Phys. Chem. C,* 2013, vol. 117, p. 1257.

13. Aurbach, D., *J. Power Sources,* 2000, vol. 89, p. 206.

14. Korusenko, P.M., Nesov, S.N., Bolotov, V.V., et al., *Nucl. Instrum. Methods Phys. Res., Sect. B,* 2017, vol. 394, p. 37.

15. Pushkarev, A.I., Isakova, Yu.I., and Khailov, I.P., *Eur. Phys. J. D,* 2015, vol. 69, p. 1.

16. Korusenko, P.M., Nesov, S.N., Bolotov, V.V., et al., *J. Alloys Compd.,* 2019, vol. 793, p. 723.

17. Fedoseeva, Yu.V., Okotrub, A.V., Bulusheva, L.G., et al., *Diamond Relat. Mater.,* 2016, vol. 70, p. 46.

18. Nesov, S.N., Korusenko, P.M., Povoroznyuk, S.N., et al., *Nucl. Instrum. Methods Phys. Res., Sect. B,* 2017, vol. 410, p. 222.

19. Wu, M., Jin, J., and Wen, Z., *RSC Adv.,* 2016, vol. 6, p. 40270.

20. Yoon, T., Chapman, N., Seo, D.M., et al., *J. Electrochem. Soc.,* 2017, vol. 164, p. A2082.

21. Bulusheva, L.G., Arkhipov, V.E., Fedorovskaya, E.O., Zhang Su, et al., *J. Power Sources,* 2016, vol. 311, p. 42.

22. Bulusheva, L.G., Okotrub, A.V., Kurenya, A.G., et al., *Carbon,* 2011, vol. 49, p. 4013.

23. He, Y., Xu, G., Wang, C., et al., *Electrochim. Acta,* 2018, vol. 264, p. 173.

Translated by D. Marinin